









Sol-Gel Synthesized Palladium-Cobalt co-doped Titanium (IV) Oxide Nanocomposite as an Efficient Photocatalyst for Removal of Dye Contamination

Abbeb Olalekan Muraina ¹ , Omonike Mary Adedokun ¹ , Maroof Alade Kareem ¹ , Khadijat Kuburat Babalola ² , Ismaila Taiwo Bello ^{1,3} , Peverga Rex Jubu ⁴ , Akeem Adekunle Adewale ^{1,5} , Oluwaseun Adedokun ^{1,5,*} 

¹ Department of Pure and Applied Physics, Ladoke Akintola University of Technology, P.M.B 4000 Ogbomoso, Nigeria; murrayabeeb@gmail.com (A.O.M); adedokunomonike@gmail.com (O.M.A.); kareemmaroof@gmail.com (M.A.K.); aaadewale38@lautech.edu.ng (A.A.A.); oadedokun@lautech.edu.ng (O.A.);

² Department of Physical and Chemical Sciences, Federal University of Health Sciences, Ila-Orangun, Nigeria; khadijat.babalola@fuhsi.edu.ng;

³ Department of Physics, College of Science, Engineering and Technology, University of South Africa, Johannesburg 1710, South Africa; ismailbello26@gmail.com;

⁴ Department of Physics, Joseph Sarwuan Tarkaa University Makurdi (JOSTUM), P.M.B. 2373, Makurdi, Benue State, Nigeria; peverga.jubu@uam.edu.ng;

⁵ Nanotechnology Research Group (NANO+), Ladoke Akintola University of Technology, Ogbomoso, Nigeria; oadedokun@lautech.edu.ng (O.A.); aaadewale38@lautech.edu.ng (A.A.A.);

* Correspondence: oadedokun@lautech.edu.ng;

Scopus Author ID 57190128209

Received: 26.02.2024; Accepted: 30.06.2024; Published: 15.02.2025

Abstract: In this study, the sol-gel technique was used to synthesize undoped, Pd-doped, Co-doped, and co-doped TiO₂ nanoparticles in order to investigate the effect of co-doping on photocatalytic activities of TiO₂. The effect of dopants on the energy band gap, charge transfer, and the recombination rate at the surface of the nanocomposite was investigated using different characterization techniques such as XRD, SEM, EDX, DRS, FTIR, and EIS. The XRD result confirmed the tetragonal structure of TiO₂ with the main diffraction peak of 25.73° at 2θ. Using Kubelka Munk's relation, the energy bandgap of the synthesized nanoparticle was obtained. The bandgap was narrowed after co-doping TiO₂ with Pd and Co, and the energy bandgap of 2.69 eV was obtained for the co-doped nanoparticles compared to the value of 3.20 eV for pure TiO₂. The SEM micrograph revealed the tetragonal structure of the nanoparticles with different sizes. The EDX results revealed the weight percentage, elemental component, and atomic concentration of the samples. The FTIR spectrum shows a predominant peak at the middle of 800 and 600 cm⁻¹, and the band is related to metal-oxygen bonds. The FTIR band at 3420 cm⁻¹ shows the presence of hydroxyl group. The EIS spectra show the capacitive behavior, which enhances the charge transport at the surface of the nanocomposite and mitigates the recombination rate. Using MB dye as the model dye to undergo photocatalytic degradation, the photocatalytic activity of the prepared samples was examined. The photodegradation efficiency of TiO₂ was enhanced as a result of Pd-doped TiO₂ nanoparticles, which showed a maximum efficiency of 96.9%.

Keywords: TiO₂ nanoparticle; nanocomposite; sol-gel; energy bandgap; photocatalyst; dye degradation.

© 2025 by the authors. This article is an open-access article distributed under the terms and conditions of the Creative Commons Attribution (CC BY) license (<https://creativecommons.org/licenses/by/4.0/>).

1. Introduction

Environmental pollution has increased rapidly as a result of the global increase in population and industrialization. Wastewater containing dyes released by the textile, food, and paper industries is one of the main pollution sources [1, 2]. These effluents contain hazardous, non-biodegradable substances that are damaging to humans, as well as carcinogenic compounds and colored pigments [3]. Numerous dyes, particularly those used in the textile industries, are released into the environment through wastewater. This has adverse impacts on natural components, like water and air, that are essential to life. Therefore, sustainable ways to reduce pollution are essential in providing a safe and clean environment for people [1].

The creation of effective methods for removing organic and inorganic contaminants from the wastewater and environment has received more attention. Industrial wastewater can be treated using various techniques, including ion exchange and adsorption, but these options are expensive, have poor degradation efficiency, and are technologically complex [4]. The use of semiconductor nanoparticles for photocatalysis has gained more attention in addressing global pollution problems. Degradation of organic contaminants in water is one of the main uses of this technology [5, 6]. Photocatalysis is a potential chemical process due to its ease of use, cheap cost, lack of toxicity, and high photocatalytic degradation efficiency in visible light. Photocatalysis using semiconductor oxides, such as TiO_2 , ZnO , and WO_3 , is a favorable, environmentally benign technique for wastewater treatment because it encourages the destruction of harmful and refractory organic contaminants [7].

Titanium dioxide (TiO_2) is considered as an excellent and superior photocatalyst among semiconductor metal oxides due to its affordability, superior stability, environmental friendliness, better oxidation ability, greater specific surface area in nanomaterial, high photocatalytic activity in visible light, and suitable capacity to start a range of organic reactions [3].

TiO_2 exists in three different crystalline forms, namely, anatase, rutile, and brookite [8–11]. For photocatalysis, anatase and rutile are the favored phases, although brookite is considered the least stable phase and is typically not utilized for photocatalysis [12]. Bulk anatase and rutile have bandgaps of 3.2 and 3.0 eV, corresponding to the wavelengths of 388 and 414 nm, respectively [13]. The anatase phase's capacity to absorb hydroxyl groups and water makes it thought to be more photocatalytically active than rutile [14]. In TiO_2 -based photocatalysis, photons with energy greater than or equal to the bandgap of TiO_2 photoexcite electrons from the valence band to the conduction band, thus creating electron-hole pairs. Organic pollutants are broken down by the generated charge carriers as they travel to the surface and interact with the pollutants.

Moreover, crystalline anatase TiO_2 can be synthesized by a variety of methods, such as thermal decomposition, chemical vapor deposition, hydrothermal synthesis, vapor-liquid-solid method, chemical co-precipitation, and sol-gel methods [15]. Among the existing techniques, the sol-gel technique is a simple method used to synthesize various oxides of metal compounds.

Due to the relatively large energy band gap of TiO_2 , photoactivation of the material is limited to ultraviolet light, which led a very low solar light utilization efficiency [16]. The bandgap energy of semiconductors is known to have a significant impact on photon absorption. Photon energy must exceed the semiconducting energy bandgap in order for the photocatalyst to absorb the photons [17]. As a result, its solar energy absorption is restricted to the ultraviolet (UV) light spectrum, which makes up only about 5% of the solar spectrum in comparison to

visible light (45%) [1,18]. In other words, a huge quantity of solar energy cannot be used because ultraviolet light only takes up a small portion of sunlight, resulting in ineffective electron transfer and poor electrical conductivity [19].

Furthermore, the rapid recombination of the photogenerated electron-hole pairs limits the photocatalytic activity of TiO₂, resulting in a low quantum yield rate and a constrained photooxidation rate [20]. Numerous strategies have been used, including incorporating TiO₂ into another low band gap semiconductor, which can activate it when exposed to visible light [1,21-22]. Thus, doping TiO₂ with either metal or non-metal or co-doping of TiO₂ with a metal and transition metal is therefore suitable for tuning the band gap while minimizing the recombination rate [23].

Doping TiO₂ with appropriate donor atoms can improve photocatalytic activity, yet because of the partially occupied impurity bands, they always function as recombination centers [24,25]. Co-doping TiO₂ with two or more atoms has been shown to theoretically passivate the impurity bands and reduce the development of recombination centers by raising the dopant's solubility limit [14]. Furthermore, co-doping can also modulate the charge equilibrium. Co-doping is a promising strategy that improves charge transfer by enhancing photocatalytic activity and reducing the rate at which the photogenerated electron-hole recombines. Co-doped TiO₂ effectively moves the absorption edge of TiO₂ from ultraviolet to visible light spectrum [26].

Chauhan *et al.* (2019) described the preparation of nitrogen and palladium co-doped mesoporous titanium dioxide nanoparticles utilizing an evaporation-induced self-assembly approach with titanium isopropoxide as a precursor of titania. The mesoporous TiO₂ nanoparticles have a crystalline size ranging from 7 to 11 nm, confirmed to occur in the tetragonal phase. The co-doped TiO₂ with Palladium and nitrogen demonstrates how an increase in the concentration of both elements causes a rapid reduction in the energy band gap and recombination rate [27].

Synthesis of cobalt and sulfur co-doped titanium dioxide nanostructures by the sol-gel method with improved photo-response characteristics for photocatalyst was reported by Jin *et al.* (2017). The photo-response range of the co-doped TiO₂ increased tremendously when compared to pure TiO₂. With an increase in the concentration of cobalt and sulfur, the grain sizes of cobalt and sulfur co-doped TiO₂ shrank, and then the catalysts had an obvious red shift in absorption of visible light. In comparison to undoped TiO₂, TiO₂ co-doped with cobalt and sulfur appears to have better degradation efficiency in the degradation of Rhodamine B [28].

In order to enhance the performance of TiO₂, we examine the influence of dopants on the energy band gaps of TiO₂ nanoparticles. We, therefore, synthesize and study the structural and optical characteristics of undoped, palladium/cobalt doped, and co-doped TiO₂ nanocomposite prepared through a simplified sol-gel method so that the synthesized material could be utilized in treating the organic pollutants present in water.

2. Material and Methods

2.1. Materials.

Titanium isopropoxide (TTIP) was employed as a precursor for TiO₂, palladium (II) nitrate and cobalt (II) acetate-tetrahydrate were used as dopants for palladium and cobalt sources, respectively, de-ionized water and 2-propanol were used as solvents and acetic acid

was used as a complexing agent for synthesis. All chemicals were of analytical grade and were used as received.

2.2. Preparation of pure TiO₂.

Pure TiO₂ nanoparticles were prepared using titanium isopropoxide or TTIP as the precursor. In this synthesis, 13 ml of 2-propanol was taken into a beaker, and 10 ml of acetic acid was added slowly. The solution was stirred for a few minutes. Afterwards, 5 ml of TTIP was added to the solution and stirred vigorously for 15 minutes. 61 ml of de-ionized water was added drop wisely within 10 minutes to the solution and stirred continuously for 4 hours. Consequently, the obtained solution was aged for 24 hours at room temperature. Then, the prepared TiO₂ gel was dried at 100°C for a few hours (at least 5 hrs) in order to obtain the desired TiO₂ nanoparticles. The obtained powder samples were ground to avoid agglomeration and to obtain a fine powder. Finally, the powder samples were annealed at 500°C for 3 hours [29].

2.3. Preparation of doped TiO₂.

For the synthesis of doped TiO₂, Palladium (II) nitrate or Cobalt (II) acetate-tetrahydrate was dissolved in 61 ml of de-ionized water at room temperature, stirred for 30 minutes to obtain a solution X. A solution Y was obtained by dissolving 5 ml of TTIP into 13 ml of 2-propanol and 10 ml of acetic acid, stirred for 30 minutes. Then, solution X was added and dropped wisely into solution Y within 10 minutes under continuous vigorous stirring. The obtained solution was stirred for 2 hours at room temperature and left to age for 24 hours. The doped TiO₂ gel was dried for some hours at 100°C, and the powder obtained was pulverized and annealed at 500°C for 3 hours [29].

2.4. Preparation of co-doped TiO₂.

Palladium nitrate and Cobalt (II) acetate-tetrahydrate were dissolved in 61 ml of de-ionized water at room temperature and stirred for 30 minutes to obtain a Solution I. Solution II was obtained by dissolving 5 ml of TTIP into 13 ml of 2-propanol and 10 ml of acetic acid, stirred for 30 minutes. Then, solution I was added and dropped wisely into solution II within 10 minutes under continuous vigorous stirring. The obtained solution was stirred for 2 hours at room temperature and left to age for 24 hours. The synthesized Pd/Co co-doped TiO₂ gel was dried for a few hours at 100°C, and the powder obtained was pulverized and annealed at 500°C for 3 hours [29].

2.5. Samples characterization.

By employing a Rigaku X-ray diffractometer (Smartlab) with an X-ray generator operating at 40 kV and 30 mA for X-ray powder diffraction, the crystalline structures and other structural properties of all powder samples were assessed. The shape, size, morphology, and dispersion of the samples were examined using scanning electron microscopy (SEM, VEGA TESCAN 3 Model) coupled with an energy - dispersive X - ray spectrometer (EDX Model INCA 200 (UK)) at 20 keV. Fourier transform infrared (FTIR) spectroscopy was performed using Model Perkin Elmer FTIR spectrometer from 4000 to 400 cm⁻¹ to examine the chemical composition and the functional group of the undoped, doped, and co-doped TiO₂ nanoparticles.

A Gamry Interface 1000 Potentiostat was used to investigate the charge transfer and recombination rate at the surface of the nanocomposite. UV–visible spectrophotometer, in conjunction with a diffuse reflectance accessory (integrating sphere), determined the optical transmittance and reflectance data for the prepared nanoparticles. An ocean optics USB 4000 spectrometer was used to record UV–vis diffuse reflectance spectra (UV–Vis DRS) in the wavelength range of 200 to 800 nm.

2.6. Photocatalytic experiment.

In order to degrade a modeled dye (methylene blue dye), the photocatalytic activity of the prepared samples was tested in the presence of sunlight. At 12:00 pm on the 20th of September, 2023, a lux meter measured a solar intensity of about 85,500 lx. Every other parameter remains the same throughout the experiment except for the sun's intensity. The MB dye solution of 2.5 mol/L was made with distilled water at neutral pH. In a volumetric flask, 1000 ml of MB solution was prepared. A 250 ml beaker serves as the reaction vessel positioned on a magnetic stirrer. 10 mg of photocatalyst was added to each 25 ml of MB dye solution, and the mixture was agitated for 20 minutes. The suspension was subjected to solar light for 60 minutes after being left in the dark for 30 minutes to allow adsorption-desorption equilibration. At a consistent solar intensity of 85,500lx, the measurements were successfully obtained. 2 ml was extracted from the solution at the predetermined intervals (0 minutes, 15 minutes, 30 minutes, 45 minutes, and 60 minutes) and centrifuged for 5 minutes for the purpose of removing the photocatalyst. A UV–visible spectrophotometer was utilized to analyze the supernatant in order to measure the absorbance and determine the degradation percentage.

3. Results and Discussion

3.1. Structural analysis.

XRD analysis was performed on all the samples to examine the crystalline structure and phase evolution of the synthesized undoped, doped, and co-doped TiO₂ nanoparticles. Figure 1 displays the XRD pattern of the prepared samples, showing the diffraction peaks, which are used to determine the materials' crystalline phase. Peak broadening was estimated using X-ray diffraction (XRD), which is related to lattice strain and particle size caused by crystal defects and dislocations [30].

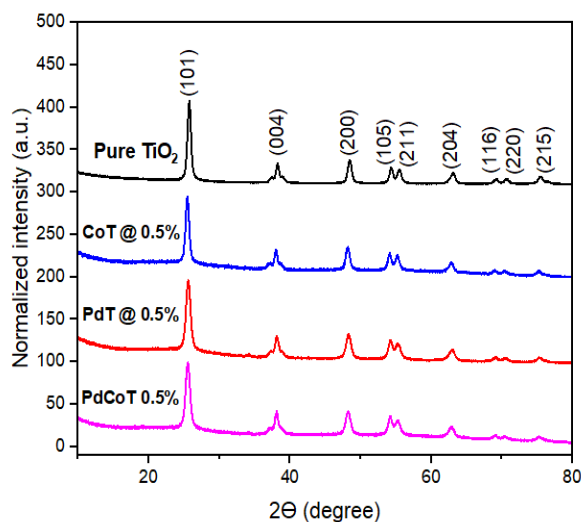


Figure 1. XRD plot of pure, doped, and co-doped TiO₂ nanoparticles.

The XRD study revealed that the diffraction peaks in each sample were ordered to the tetragonal anatase phase of titanium corresponding to JCPDS [Card No: 84-1285]. The diffraction peaks morphology of pure TiO₂ crystal planes shown in Figure 1 is fairly similar to that of Pd and Co-doped TiO₂, which is in good agreement with other experimental work [31].

The peak locations and the relative intensities of the prepared samples in XRD patterns are in agreement with the anatase TiO₂ standard powder diffraction patterns. The pattern pronounced the main diffraction peak at 25.73° corresponding to the (101) plane. The anatase displays a distinct tetragonal structure at 38.27°, 48.48°, 54.36°, 55.48°, 63.09°, 69.22°, 70.71° and 75.50° aligning with the diffraction planes (004), (200), (105), (211), (204), (116), (220), and (215) respectively are in accordance with the TiO₂ anatase phase according to JCPDS [No: 84-1285]. The average crystallite sizes were obtained from the full width at half-maximum (FWHM) of the diffraction peaks via Scherrer's equation:

$$D = \frac{K\lambda}{\beta \cos \theta} \quad (1)$$

Where K is the shape factor, taken as 0.9, θ is the Bragg's (peak) angle, λ is the wavelength, β is the diffraction peak's full width at half-maximum (FWHM) in radian, and D is the crystallite size. The mean crystalline size of the anatase was obtained to be 14.32 nm. The synthesized samples were presented in Table 1 with their corresponding concentrations, crystal sizes, and FWHM.

Table 1. Relationship between crystal sizes and FWHM of the prepared nanoparticles.

Samples	Concentrations (%)	Crystal Sizes (nm)	FWHM (degree)
Pure TiO ₂	0.00	15.93	0.5533
Pd doped TiO ₂	0.50	12.59	0.6952
Co-doped TiO ₂	0.50	15.85	0.5540
Pd and Co co-doped TiO ₂	0.50	12.90	0.6821

3.2. Morphological analysis.

Researchers have investigated doping and co-doping effects on TiO₂ using a field emission scanning electron microscope (FESEM). This has been applied to the study of morphological characteristics, such as the shapes and sizes of the synthesized materials. With the aid of backscattered or secondary electrons, FESEM enables imaging of a solid surface's topography. Figures 2 (a-d) reveal the morphological images of undoped TiO₂, palladium-doped TiO₂, Cobalt-doped TiO₂, and Palladium/Cobalt co-doped TiO₂. The existence of agglomeration was clearly evident in the micrograph. Figure 2 shows an increase in the agglomeration and particle size for doped and co-doped TiO₂ [2].

Figures 3(a-d) display the elemental composition of the specified samples as shown by the EDX spectrum. Pure TiO₂ only includes the elements oxygen (O) and titanium (Ti), as confirmed by the energy dispersive x-ray spectroscopy technique. Since no additional element is present, the samples' purity is confirmed. Palladium-doped TiO₂ encloses titanium (Ti), oxygen (O), and palladium (Pd); cobalt-doped TiO₂ displays the existence of titanium (Ti), oxygen (O), and cobalt (Co), whereas Pd/Co co-doped TiO₂ encompasses of titanium (Ti), oxygen (O), cobalt (Co) and palladium (Pd) as displaced in Figure 3, indicating that Pd and Co are effectively integrated into TiO₂. These spectra can confirm the elements related to the host and dopants and the atomic and weight percentages used to evaluate the element's stoichiometry [29]. The inset in Figure 3 displayed the atomic and weight percentage of pure, doped, and co-doped TiO₂ as revealed by the EDX spectra.

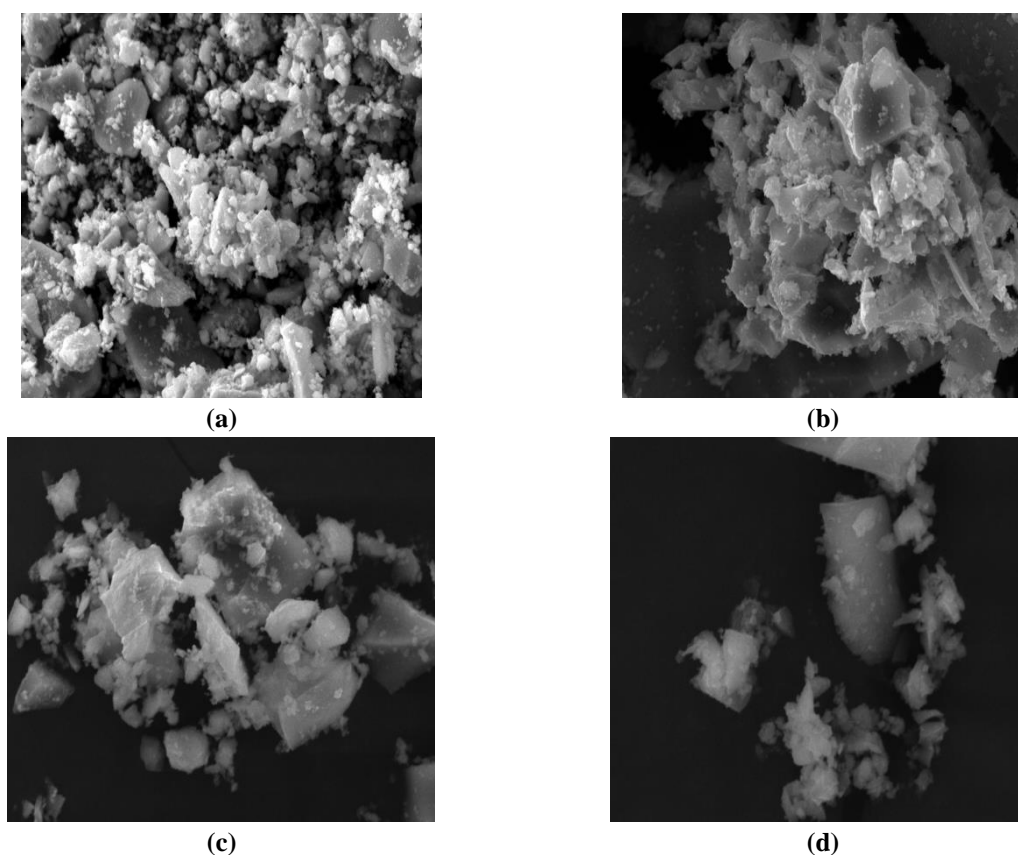


Figure 2. SEM images of (a) pure TiO₂; (b) Pd-doped TiO₂; (c) Co-doped; (d) Co-doped TiO₂.

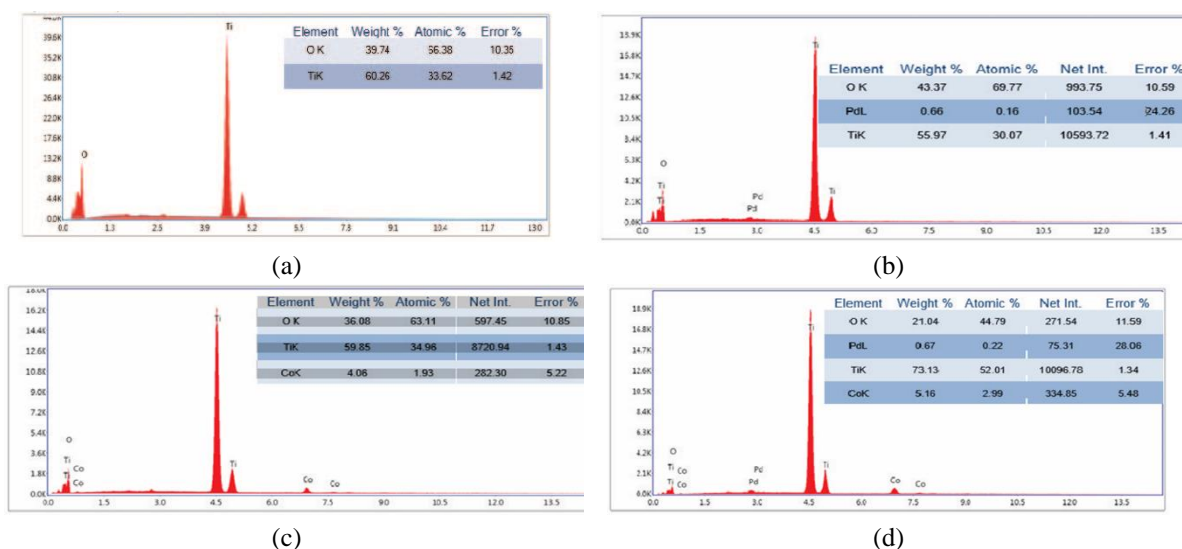


Figure 3. EDX spectrum of (a) pure TiO₂; (b) Pd-doped TiO₂; (c) Co-doped; (d) Co-doped TiO₂.

3.3. FTIR analysis.

From FTIR analysis, the chemical composition and functional group of the prepared samples were verified. The FT-IR spectra obtained for the synthesized pure TiO₂, palladium-doped TiO₂, cobalt-doped TiO₂, and palladium/cobalt co-doped TiO₂ are presented in Figure 4.

As Table 2 illustrates, distinct peaks were found for several functional groups. The IR spectrum of pure TiO₂ nanoparticles exhibits bands at 3412, 1620, 738, and 472 cm⁻¹. The presence of peaks between 1700 and 1600 cm⁻¹ indicates the stretching vibration of the hydroxyl groups on the surface and interlayer.

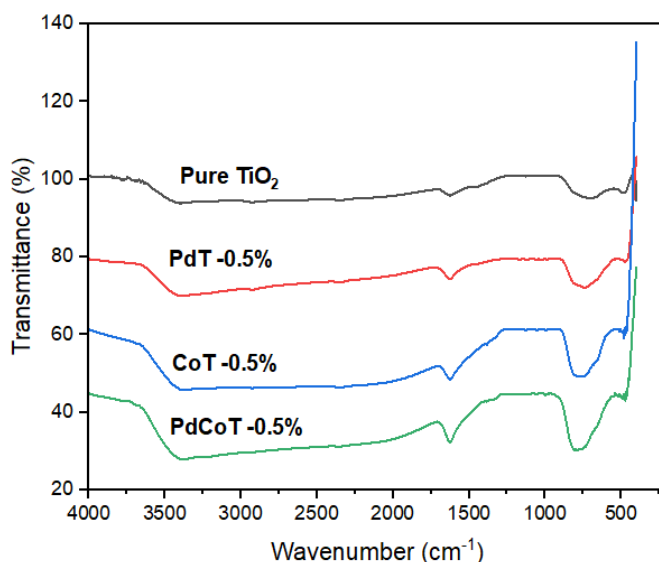


Figure 4. Fourier transform infrared spectra for pure, doped, and co-doped TiO₂.

The formation of hydroxyl radicals in a photocatalytic system depends on hydroxyl groups [32]. The O-H stretching vibration, which displays a hydroxyl group, was identified as the of the FTIR band at 3412 cm⁻¹. A prominent peak that appeared at the middle of 800 and 600 cm⁻¹ FTIR bands was associated with metal-oxygen bonding, and this finding is consistent with other experimental work. The FTIR absorption values for the samples were presented in Table 2 with their functional group.

Table 2. FTIR Absorption value for undoped, doped, and co-doped TiO₂.

Wavenumber (cm ⁻¹)	Pure TiO ₂	PdT	CoT	PdCoT	Functional group
3550 - 3200	3412	3415	3415	3417	O-H
1680 - 1620	1620	1624	1625	1628	C=C
900 - 680	738	740	775	800	C-H
< 600	472	472	476	480	C-I

3.4. Optical studies.

A UV-Vis spectrophotometer operating in diffuse reflectance scattering (DRS) at room temperature was used to evaluate the optical properties of the prepared samples. Figure 5(a) shows the absorption spectra of the samples in the scanning range of 200-800 nm.

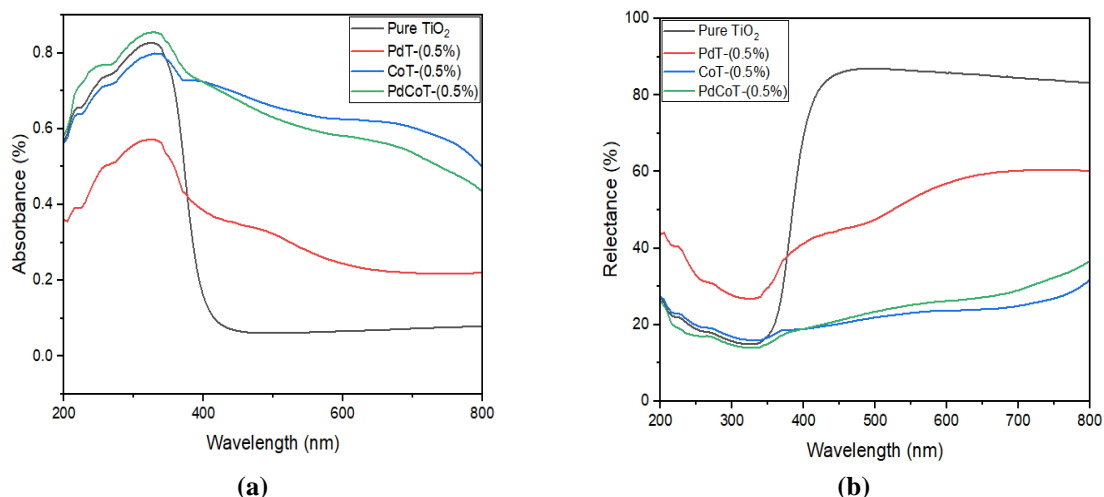


Figure 5. DRS spectra of (a) absorbance; (b) reflectance for pure, doped, and co-doped TiO₂ nanoparticles.

For unmodified TiO₂, a wide absorbance band for the wavelength range of about 400 nm can be observed, indicating that its photoactivity is limited to the UV region of the spectrum. The UV–vis spectrum (Figure 5(a)) demonstrates that samples absorb in the 225–360 nm spectral region. The undoped TiO₂ spectrum showed that maximal absorption happened at 328 nm.

Subsequently, Pd-doped TiO₂, Co-doped TiO₂, and Co/Pd co-doped TiO₂ caused the photo-absorption edge to move slightly to the higher wavelengths of 330, 332, and 335 nm, respectively. This showed that compared to undoped TiO₂, doping Palladium and Cobalt with TiO₂ nanoparticles resulted in significantly higher absorption of visible and ultraviolet light. There is a shift in the absorption band for the doped and the co-doped TiO₂. This trend of increasing wavelength on doping into TiO₂ shows a shift from the UV region to the visible light region. The shift resulted from the incorporation of dopants with TiO₂ nanoparticles. The shifts of this type could be attributed to the charge-transfer transitions between the electrons of the doped samples and the TiO₂ conduction or valence band.

Diffuse reflectance spectra (DRS) of undoped TiO₂, as well as doped and co-doped TiO₂ nanoparticles against wavelength, are shown in Figure 5(b). The reflectance that arises in the optical transitions is what causes the significant peak observed at about 400 nm. DRS provides an accurate identification of such impurities since the diffuse reflectance is extremely sensitive to small modifications [33]. From the reflectance data acquired by diffuse reflectance spectrometry, the optical band-gap was calculated. By using the Tauc graphical approach to examine the optical characteristics of the nanocomposite, the energy gap of the samples was ascertained. The band-gap estimated from the diffused reflectance spectra was determined through a Tauc plot [graph of $(F(R)h\nu)^2$ against the photon energy ($h\nu$)] for the direct transition plot as presented in Figure 6.

$$F(R) = \frac{K}{S} = \frac{(1-R)^2}{2R} \quad (2)$$

Where $F(R)$ is called the Kubelka Munk function, R is the diffuse reflectance of the sample, S represents the scattering coefficient, and K is the corresponding K-M absorption.

By plotting the equation $(F(R)h\nu)^2$ versus $h\nu$, the band-gap of the semiconductor was obtained. The calculated band-gap of TiO₂ decreases significantly from 3.20 eV to 2.98 eV for palladium modification. Also, the band-gap of cobalt doping indicates 2.79 eV, while Pd/Co co-doping shows 2.69 eV.

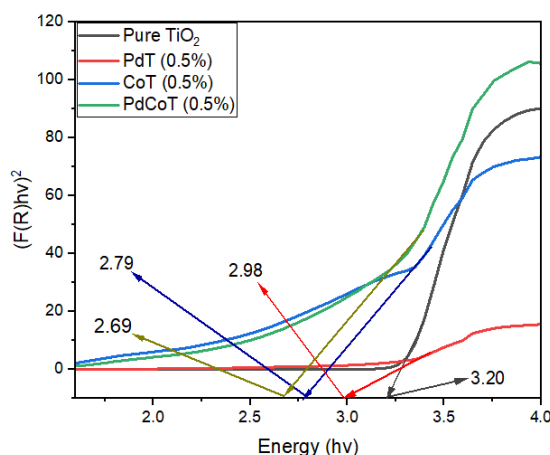


Figure 6. Plot of $(F(R)h\nu)^2$ against energy ($h\nu$) for pure, doped, and co-doped TiO₂.

The band gap of the doped materials shifted from the UV region to visible light, which implies that the shift of absorption spectrum is attributed to the band gap narrowing, probably

due to the dopants present in the material. The disparity in band gap values observed in Figure 6 with Pd/Co doping of TiO₂ is caused by the presence of oxygen vacancies, which facilitate the easier transfer of electrons from the valence band to the conduction band [34]. The effective reduction in the optical band gap could improve the photocatalytic performance of the doped material.

3.5. EIS analysis.

The prepared samples were further examined by electrochemical impedance spectroscopy (EIS) to reveal details about the interfacial properties, such as the charge transfer resistance of the conductive layer, as indicated by the Nyquist plot. This method suggests an electrochemical approach to examine charge transport and recombination rate at the TiO₂ interface. The resulting Nyquist plot of the real and the imaginary parts of the impedance and equivalent circuit model for fitted data are shown in Figure 7.

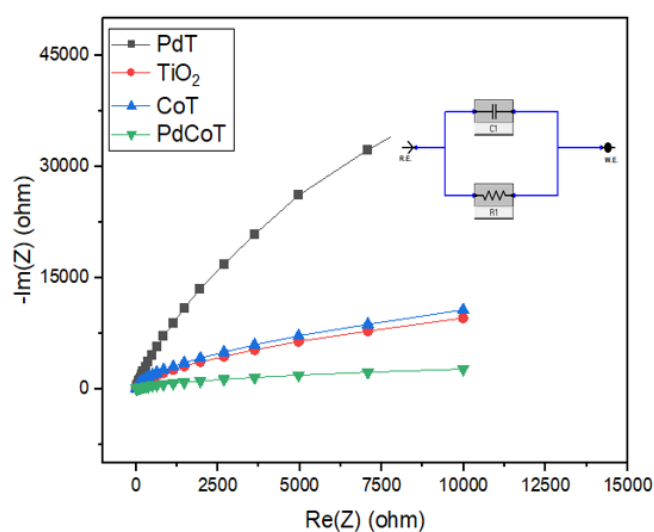


Figure 7. The Nyquist plot of pure, doped, and co-doped TiO₂.

At the electrode interface, an electron is transferred during an electrochemical process. The obtained EIS spectra indicate the charge transfer process at the maxima of the curve in a high-frequency region. The diameter of the Nyquist plot's curve was utilized to evaluate the charge electron-transfer resistance.

The doping of Pd with TiO₂ resulted in a reduction in the diameter of the high-frequency curve, indicating a lower charge recombination resistance in the sample. Also, the significant decrease demonstrated the dopants' advantage in enhancing electron transport and reducing electron-hole recombination [35]. Furthermore, palladium-doped TiO₂ exhibits capacitive behavior, as revealed in the Nyquist plot, which enhances the movement of charge at the nanocomposite's surface and mitigates the recombination rate.

3.6. Photocatalytic degradation of MB.

The synthesized nanoparticles could be used as a photocatalyst to turn the aqueous methylene blue (MB) contaminated in water into a colorless form under visible light. The photocatalytic degradation of methylene blue (MB) was observed under direct sunlight. Figures 8(a-d) displays the results of the UV-Vis absorbance spectrum of the photocatalytic degradation of methylene blue in the presence of sunlight.

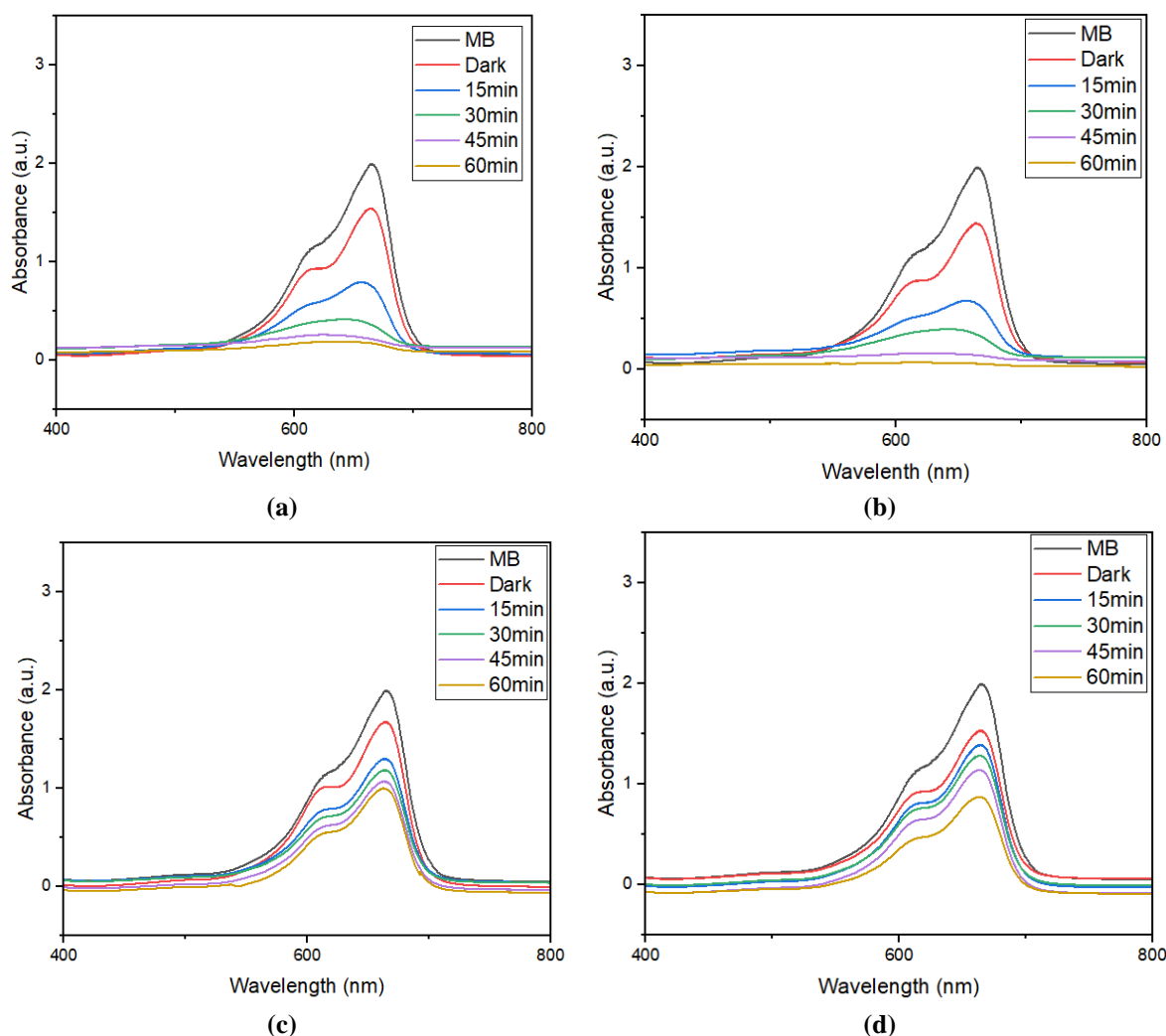


Figure 8. MB solution’s absorbance spectra for (a) pure TiO₂; (b) Pd-doped TiO₂; (c) Co-doped TiO₂; (d) Pd/Co co-doped TiO₂ under solar irradiation.

At room temperature, a UV-visible spectrophotometer with a wavelength range of 200–800 nm was used to monitor the reaction. The UV–visible absorbance spectrum of methylene blue dye solution shows the maximum absorbance at 665 nm. The absorbance peak continues to decrease as the irradiation time increases when the photocatalyst and sunlight are present.

Even though pure TiO₂ outperforms cobalt-doped TiO₂ samples due to photon scattering caused by excess cobalt concentration [36], in addition, Hamadianian *et al.* (2010), have better photocatalytic activity of undoped TiO₂ compared to Co-doped TiO₂ in the degradation of methyl orange under UV irradiation [37]. According to the report of Liang and his colleagues in 2016, the photocatalytic rate of undoped titanium dioxide was higher than Cobalt-doped TiO₂ for larger cobalt concentrations (exceeding 2.5%). This occurs because excess cobalt dopants lead to photon scattering [38]. In comparison to undoped TiO₂ and Cobalt-doped TiO₂ nanoparticles, palladium-doped TiO₂ decolorizes the MB dye solution faster. Throughout the process of degradation, the bright blue of the MB dye solution gradually diminished and became colorless. It was observed that Pd-doped TiO₂ degraded MB dye solution after 60 minutes, which proved that palladium has the best performance in the photocatalytic degradation of MB among all the samples used [5]. The percentage degradation of the dye was displayed in Figure 9, which was calculated using the equation:

$$\% \text{ Degradation} = \frac{C_0 - C_t}{C_0} \times 100 \quad (3)$$

Where C_o is the initial concentration of MB dye, C_t is the concentration of MB dye solution after exposure time (t) to solar radiation.

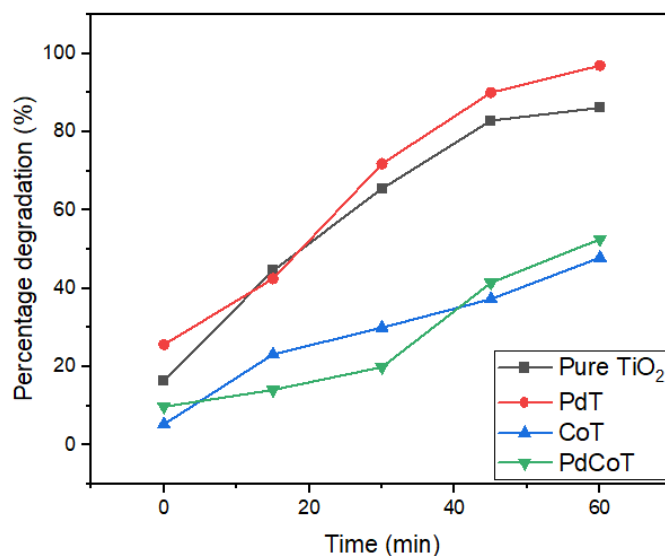


Figure 9. The percentage degradation plot for pure TiO₂, Pd-doped TiO₂, Co-doped TiO₂, and Pd/Co co-doped TiO₂.

The photocatalytic degradation was found to increase linearly as the irradiation time increased. The recorded adsorption of undoped, Pd-doped, Co-doped, and Pd/Co co-doped TiO₂ are 16.48, 26.85, 6.59, and 9.89%, respectively, after 30 minutes of agitating the dye solution in a dark environment. The final degradation percentages of the MB dye with undoped, Pd-doped, Co-doped, and co-doped TiO₂ were 86.18, 96.98, 47.89, and 52.65% respectively. The photodegradation efficiency of TiO₂ was enhanced as a result of Pd-doped TiO₂ nanoparticles, which showed a maximum efficiency of 96.98%. Pd-doped samples are better than other samples so that they can be used for environmental applications. The photodegradation efficacy of the current work and the previously reported work is displayed in Table 3. This current study exhibits better performance with shorter exposure time and a dye degradation percentage of 96.9%.

Table 3. Comparison of the present work with the literature.

S/N	Samples	Dye	Degradation (%)	Time (min)	References
1.	N/Pd-codoped TiO ₂ (5% N and 8% Pd)	MB	78	90	[19]
2.	Co/S codoped TiO ₂ (2% Co and 5% S)	RhB	30	100	[20]
3.	N/Pd-codoped TiO ₂ (0.6% Pd)	Eosin Yellow	100	180	[4]
4.	N/Pd and Ag-doped TiO ₂ (5%N, 3% Pd and 6%Ag)	MB	92	120	[39]
5.	Pd-doped TiO ₂ (0.5%)	MB	99.4	120	[40]
6.	Co-S co-doped TiO ₂ (1%)	Malachite Green	20	50	[41]
7.	Pd doped TiO ₂ (0.5%)	MB	96.9	60	Present work

3.6. Proposed photocatalytic mechanism.

Figure 10 illustrates the photogenerated charge carriers' mechanism, migration, and degradation process in the presence of sunlight. Based on the separation process of the photogenerated electron-hole charge carriers, the Pd-doped TiO₂ nanoparticle photocatalytic mechanism was proposed. The photogenerated electrons are trapped, which leads to electron-hole separation. When photons strike TiO₂, they produce electrons that migrate from the

valence band (VB) to the conduction band (CB) and leave holes behind in the valence band. The holes can produce strongly reactive hydroxyl radical species by scavenging surface-adsorbed water or hydroxyl molecules. On the other hand, the electrons react with the oxygen molecules to produce very reactive superoxide radicals, which are advantageous for mineralizing methylene blue dye-contaminated water.

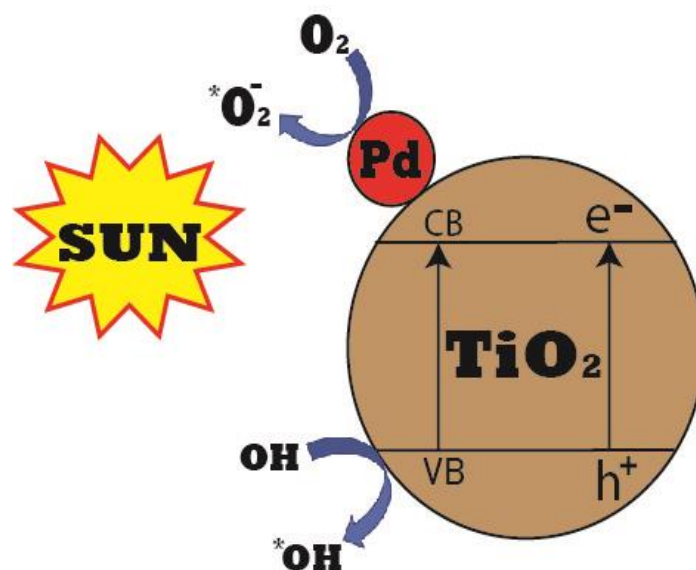


Figure 10. Photocatalytic mechanism of Pd doped TiO₂ nanoparticle.

4. Conclusion

Undoped TiO₂, palladium TiO₂, cobalt-doped TiO₂, and palladium/cobalt co-doped TiO₂ were successfully synthesized by sol-gel method. The doping and co-doping of Pd and Co into TiO₂ lattice were demonstrated in the XRD spectrum, and Pd/Co co-doping dramatically changed the optical characteristics of TiO₂ nanoparticles, reducing the level of the energy band gap from 3.20 eV to 2.69 eV. The band gap of the doped materials shifted from the UV region to the visible light region, which implies that the shift of absorption spectrum is attributed to the band gap narrowing, probably due to the dopants present in the material. EIS analysis revealed the charge transfer rate at the surface of the nanocomposite, while the functional groups of each nanoparticle were verified using FTIR spectroscopy. The significant photocatalytic activity of undoped, Pd-doped, Co-doped, and co-doped TiO₂ nanoparticles towards MB dye solutions was found to be 88, 96, 43, and 53 %, respectively. It was discovered that Pd doping significantly increased the photocatalytic activity of TiO₂ towards the degradation of MB dye in the presence of sunlight, and this resulted in a good performance with literature. In this regard, integrating Pd with TiO₂ helps nanoparticles become more photocatalytically active, and it might be one of the most effective options among available materials for treating organic pollutants in water.

Funding

This research received no external funding.

Acknowledgments

OA gratefully acknowledges the Department of Science & Technology (Govt. of India) for the award of the 2019/2020 Research Training Fellowship for Developing Countries Scientist

(RTF-DCS). The authors acknowledge with gratefulness the Centre for High-Pressure Research, Bharathidasan University, India, for sample characterizations.

Conflicts of Interest

The authors declare no conflict of interest.

References

1. Moma, J.; Baloyi, J. Modified Titanium Dioxide for Photocatalytic Application. *Intech*. **2018**, *11*, 38, <http://dx.doi.org/10.5772/intechopen.79374>.
2. Siddiqua, A.; Hahladakis, J.N.; Al-Attiya, W.A. An Overview of the environmental pollution and health effects associated with waste landfilling and open dumping. *Environ Sci Pollut Res*. **2022**, *29*, 58514–58536, <https://doi.org/10.1007/s11356-022-21578-z>
3. Hafeez, M.; Afyaz, S.; Khalid, A. Synthesis of cobalt and sulphur doped titanium dioxide photocatalysts for environmental applications. *J King Saud Univ - Sci*. **2022**, *34*, 102028, <https://doi.org/10.1016/j.jksus.2022.102028>.
4. Rani, A.; Dhiman, R.L.; Singh, V. Photocatalytic study of Ni-N-codoped TiO₂ nanoparticles under visible light irradiation. *Nano Express* **2021**, *2*, <https://doi.org/10.1088/2632-959X/abe058>.
5. Kuvarega, A.T.; Krause, R.W.M.; Mamba, B.B. Nitrogen/palladium-codoped TiO₂ for efficient visible light photocatalytic dye degradation. *J Phys Chem C*. **2011**, *115*, 22110–22120, <https://doi.org/10.1021/jp203754j>.
6. El Sharkawy, H.M.; Shawky, R.E.; Selim, H. Efficient photocatalytic degradation of organic pollutants over TiO₂ nanoparticles modified with nitrogen and MoS₂ under visible light irradiation. *Sci Rep*. **2023**, *13*, 8845, <https://doi.org/10.1038/s41598-023-35265-7>
7. Kumari, H.; Suman, S.; Ranga, R.; Chahal, S. A Review on Photocatalysis Used For Wastewater Treatment: Dye Degradation. *Springer International Publishing*. **2023**, *243*, 1-46, <https://doi.org/10.1007/s11270-023-06359-9>.
8. Ahmed, A.; Abd El-Raady, Asmaa, A.; Khodari, M.N.R. Synthesis of pure and palladium doped TiO₂ and their applications as modifiers for carbon paste electrode. *Aswan Univ J Environ Stud*. **2022**, *3*, 267–283, <https://doi.org/10.21608/aujes.2022.145415.1076>.
9. Allen, N.S.; Mahdjoub, N.; Vishnyakov, V.; The effect of crystalline phase (anatase, brookite and rutile) and size on the photocatalytic activity of calcined polymorphic titanium dioxide (TiO₂). *Polym Degrad Stab*. **2018**, *150*, 31–36, <https://doi.org/10.1016/j.polymdegradstab.2018.02.008>.
10. Shittu, H.A.; Bello, I.T.; Kareem, M.A.; Awodele, M.K.; Sanusi, Y.K.; Adedokun, O. Recent developments on the photoanodes employed in dye-sensitized solar cell. *Mater Sci Eng*. **2020**, *805*, <https://doi.org/10.1088/1757-899X/805/1/012019>.
11. Olalekan M.A.; Kareem, M.A.; Adedokun, O.; Bello, I.T. Recent Advances in Photo-supercapacitor: A Mini Review. *Advanced Materials Science and Technology* **2022**, *4*, <https://doi.org/10.37155/2717-526X-0402-2>.
12. Zhang, J.; Xu, Q.; Feng, Z. Importance of the relationship between surface phases and photocatalytic activity of TiO₂. *Angew Chemie - Int Ed* **2008**, *47*, 1766–1769, <https://doi.org/10.1002/anie.200704788>.
13. Dette, C.; Pérez-Osorio, M.A.; Kley, C.S. TiO₂ anatase with a bandgap in the visible region. *Nano Lett*. **2014**, *14*, 6533–6538, <https://doi.org/10.1021/nl503131s>.
14. Wang, H.; Huang, X.; Li, W. TiO₂ nanoparticle decorated carbon nanofibers for removal of organic dyes. *Colloids Surfaces A Physicochem Eng Asp*. **2018**, *549*, 205–211, <https://doi.org/10.1016/j.colsurfa.2018.04.017>.
15. Jeantelot, G.; Ould-Chikh, S.; Sofack-Kreutzer, J.; Morphology control of anatase TiO₂ for well-defined surface chemistry. *Phys Chem Chem Phys*. **2018**, *20*, 14362–14373, <https://doi.org/10.1039/c8cp01983e>.
16. Li, L.; Chen, X.; Quan, X.; Qiu, F.; Zhang, X. Synthesis of CuO_x/TiO₂ Photocatalysts with enhanced Photocatalytic Performance. *ACS Omega*. **2023**, *8*, 2723–2732, <https://doi.org/10.1021/acsomega.2c07364>
17. Huang, F.; Yan, A.; Zhao, H. Influences of Doping on Photocatalytic Properties of TiO₂ Photocatalyst. **2016**, <http://dx.doi.org/10.5772/63234>.
18. Szczepanik, B. Applied Clay Science Photocatalytic degradation of organic contaminants over clay-TiO₂ nanocomposites: A review. *Appl Clay Sci*. **2017**, *141*, 227–239, <https://doi.org/10.1016/j.clay.2017.05.017>.

- <https://doi.org/10.1016/j.clay.2017.02.029>.
19. Katoh, R.; Furube, A. Journal of Photochemistry and Photobiology C : Photochemistry Reviews Electron injection efficiency in dye-sensitized solar cells. " *Journal Photochem Photobiol C Photochem Rev.* **2014**, *20*, 1–16, <https://doi.org/10.1016/j.jphotochemrev.2014.02.001>.
 20. Li, N.; Zhang, W.; Wang, D.; Li, G.; Zhao, Y. Synthesis and applications of TiO₂ based Nanostructures as Photocatalytic Materials. *Chem. Asian.* **2022**, *17*, e202200822, <https://doi.org/10.1002/asia.202200822>.
 21. Hossain, K.; Hossain, M.; Akhtar, S. Studies on synthesis, Characterization, and Photocatalytic activity of TiO₂ and Cr-doped TiO₂ for the degradation of p-chlorophenol. *ACS Omega.* **2023**, *8*, 1979-1988, <https://doi.org/10.1021/acsomega.2c05107>.
 22. Azem, F.A.K.; Birlik, I.; Keskin, O.Y.; Delice, T.K. Improvement of photocatalytic degradation of Titanium dioxide nanomaterials by non-metal doping. *AKU J. Sci. Eng.* **2023**, 874-882, <https://doi.org/10.35414/akufemubid.1256778>.
 23. Orizu, G.E.; Ugwuoke, P.E; Asogwa, P.U.; Offiah, S.U. A review on the inference of doping TiO₂ with metals/non-metals to improve its photocatalytic activities. *Earth Environ. Sci.* **2023**, *1178*, 012008, <https://doi.org/10.1088/1755-1315/1178/1/012008>.
 24. Mragui, A.E.I.; Logvina, Y.; Zegaoui, O.; Esteves, J.C.G. Photocatalytic Activity Under Visible Irradiation Toward Carbamazepine Degradation. *Materials* **2019**, *12*, 3874, <https://doi.org/10.3390/ma12233874>.
 25. Wahyuni, E.T.; Lestari, N.D.; Cinjana, I.R. Doping TiO₂ with Fe from iron rusty waste for enhancing its activity under visible light in the Congo red dye photodegradation. *J. Eng. Appl. Sci.* **2023**, *70*, 9, <https://doi.org/10.1186/s44147-023-00178-9>.
 26. Wen, C.; Zhu, Y.J.; Kanbara. T. Effects of I and F codoped TiO₂ on the photocatalytic degradation of methylene blue. *Desalination.* **2009**, *249*, 621–625, <https://doi.org/10.1016/j.desal.2009.01.028>.
 27. Chauhan, N.; Singh, V.; Kumar, S. Synthesis of nitrogen & palladium co-doped mesoporous titanium dioxide nanoparticles via evaporation induced self assembly method and study of their photocatalytic properties. *J Mol Struct.* **2019**, *1185*, 219–228, <https://doi.org/10.1016/j.molstruc.2019.02.055>.
 28. Jin, Q.; Nie, C.; Shen Q.; Xu, Y.; Nie, Y. Cobalt and sulfur co-doped TiO₂ nanostructures with enhanced photo-response properties for photocatalyst. *Funct Mater Lett.* **2017**, *10*, 1–4, <https://doi.org/10.1142/S1793604717500618>.
 29. Adedokun, O.; Sivaprakash, P.; Ajani, A.S.; Bello, I.T.; Arumugam, S. Structural, optical and magnetic studies of sol-gel synthesized Mg-doped pure anatase TiO₂ nanoparticles for spintronic and optoelectronics applications. *Phys B Condens Matter.* **2023**, *667*, 415199, <https://doi.org/10.1016/j.physb.2023.415199>.
 30. Yogamalar, R.; Srinivasan, R.; Vinu, A. X-ray peak broadening analysis in ZnO nanoparticles. *Solid State Commun.* **2009**, *149*, 1919–1923, <https://doi.org/10.1016/j.ssc.2009.07.043>.
 31. Abd El-Rady, A.A.; Abd El-Sadek M.S., El-Sayed Breky, M.M.; Assaf, F.H. Characterization and Photocatalytic Efficiency of Palladium Doped-TiO₂ Nanoparticles. *Adv Nanoparticles* **2013**, *02*, 372–377, <https://doi.org/10.4236/anp.2013.24051>.
 32. Parrino, F.; Livraghi, S.; Giamello, E. Role of Hydroxyl , Superoxide , and Nitrate Radicals on the Fate of Bromide Ions in Photocatalytic TiO₂ Suspensions. *ACS Catal.* **2020**, 7922–7931, <https://doi.org/10.1021/acscatal.0c02010>.
 33. Bock, S.; Kijatkin, C.; Berben, D.; Imlau, M. Absorption and remission characterization of pure, dielectric (nano-)powders using diffuse reflectance spectroscopy: An end-to-end instruction. *Appl Sci.* **2019**, *9*, <https://doi.org/10.3390/APP9224933>.
 34. Kareem, M.A.; Bello, I.T.; Shittu, H.A.; Sivaprakash, P.; Adedokun, O.; Arumugam, S. Synthesis, characterization, and photocatalytic application of silver doped zinc oxide nanoparticles. *Clean Mater.* **2022**, *3*, 100041, <https://doi.org/10.1016/j.clema.2022.100041>.
 35. Nguyen, T.M.H.; Bark, C.W. Synthesis of Cobalt-Doped TiO₂ Based on Metal-Organic Frameworks as an Effective Electron Transport Material in Perovskite Solar Cells. *ACS Omega* **2020**, *5*, 2280–2286, <https://doi.org/10.1021/acsomega.9b03507>.
 36. Pirbazari, A.E.; Monazzam, P.; Kisomi, B.F. Co/TiO₂ nanoparticles: Preparation, characterization and its application for photocatalytic degradation of methylene blue. *Desalin Water Treat.* **2017**, *63*, 283–292, <https://doi.org/10.5004/dwt.2017.20205>.
 37. Hamadianian, M.; Reisi-Vanani, A.; Majedi, A. Sol-gel preparation and characterization of Co/TiO₂ nanoparticles: Application to the degradation of methyl orange. *J Iran Chem Soc.* **2010**, *7*, <https://doi.org/10.1007/bf03246184>.
 38. Liang, J.; Hao, C.; Yu, K.; Li, Y. Excellent photocatalytic performance of cobalt-doped titanium dioxide

- nanotubes under ultraviolet light. *Nanomaterials and Nanotechnology*. **2016**, *6*, 1–5, <https://doi.org/10.1177/1847980416680808>.
39. Chauhan, N.; Singh, V.; Kumar, S.; Sirohi, K.; Preparation of Palladium, silver, and nitrogen co-doped mesoporous titanium dioxide nanoparticles to investigate their photocatalytic action. *Mater. Res. Express*. **2019**, *6*, <https://doi.org/10.1088/2053-1591/ab50a7>.
 40. Nguyen, C.H.; Fu, C.; Juang, R. Degradation of methylene blue and methyl orange by palladium-doped TiO₂ photocatalysis for water reuse: Efficiency and degradation pathways. *J Clean Prod*. **2018**, <https://doi.org/10.1016/j.jclepro.2018.08.110>.
 41. Siddiqa, A.; Masih, D.; Anjum, D.; Siddiq, M. Cobalt and sulfur co-doped nano-size TiO₂ for photodegradation of various dyes and phenol. *Journal of Environmental Sciences* **2015**, *37*, 100-109, <https://doi.org/10.1016/j.jes.2015.04.024>.